RSC Publishing Faraday Discussions

Hot electron science and microscopic processes in plasmonics and catalysis

Journal:	*Faraday Discussions*
Manuscript ID	FD-ART-01-2019-000001
Article Type:	Paper
Date Submitted by the Author:	03-Jan-2019
Complete List of Authors:	Halas, Naomi; Rice University, Department of Electrical and Computer Engineering

Spiers Memorial Lecture

Hot electron science and microscopic processes in plasmonics and catalysis

N. J. Halas

Department of Electrical and Computer Engineering, Department of Physics and Astronomy, Department of Chemistry, Laboratory for Nanophotonics, Smalley-Curl Institute, and Department of Materials Science and NanoEngineering, Rice University, 6100 Main Street, Houston, Texas 77005, United States

Abstract

In this lecture we discuss the generation of nonequilibrium electrons in metals, their properties, and how they can be utilized in two emerging applications: for extending the capabilities of photodetection, and for photocatalysis: lowering the barriers of chemical reactions. Because direct illumination of noble/coinage metal nanoparticles results in the excitation of their localized surface plasmons, these nanostructures can serve as active optical antennas, central to the goal of efficient hot electron generation to drive these processes. Currently, noble/coinage metal nanoparticles are being supplemented by earth-abundant, sustainable alternatives. Here we discuss how active optical antennas can expand the wavelength accessibility and alter the properties of traditional photoconductive detectors in new ways. We also examine how active optical antennas, when combined with conventional catalytic nanoparticles in an integrated manner, can convert catalysts into photocatalysts to change chemical product specificities and even alter chemical reaction pathways.

Introduction

The topic of this, the 300th Faraday Discussion, lies at the confluence of electricity, chemistry, and nanoscience, a region of interest that owes a great deal to Faraday himself. Metals are appreciated for their ability to conduct electricity, a phenomenon that Faraday took advantage of with his invention of the electrical motor (alternator) in 1831, the first reliable method for generating electrical current. Prior to that, as a chemist working with Humphry Davy, his interest in how chemical reactions could induce electrical currents provided much of the foundation of electrochemistry and the design of electrical batteries. Even metal nanoparticles and their interaction with light captured Faraday's attention: he was the first scientist to realize that the optical properties of gold were dramatically transformed from reflection into the absorption of green light, once the metal was reduced in dimension to size scales far smaller than an optical wavelength. Our modern understanding of electrons that follow Fermi-Dirac statistics has spawned interest in phenomena associated with electron populations driven out of equilibrium in metals, where optical excitation can give rise to electrons with energies as high as the energy of the photon that excited them. While photons with energies greater than the work function of a metal result in electrons that are photoemitted from the metal into vacuum, the regime where electrons in a metal are excited but have insufficient energy for photoemission provides its own distinct phenomena. Here visible light can excite electrons at a metal-semiconductor interface that can traverse an interfacial barrier, or that can tunnel into an unoccupied energy level of a molecule adsorbed at the metal surface. To study and ultimately exploit this regime of electron behavior, however, requires that

nonequilibrium electrons be excited efficiently. While in bulk metals, the direct optical excitation of hot electrons is an inefficient process, the excitation of surface plasmons can result in the generation of hot electrons through plasmon decay. In metallic structures of subwavelength dimension or in periodic arrays, surface plasmons can be easily excited by direct optical illumination.[1] In other words, the direct optical excitation of surface plasmons by illuminating specific types of metallic structures provides an efficient mechanism for the generation of nonequilibrium, or "hot" electrons (and holes).

The development of metal nanoparticles and nanostructures specifically for the direct optical excitation of surface plasmons- the coherent oscillation of electrons within the metal- has been the topic of intense research activity during the past two decades, and, as an extremely active and dynamic field, has been reviewed extensively.[2-16] Much of the earlier research on this topic focused on the dependence of the plasmonic properties of nanostructures on their shape, size, and dielectric environment, primarily for sensing applications.[17-21] The intense near field that can be generated in the junction between two metallic nanostructures in close proximity to each other when appropriately illuminated has been shown to give rise to surface-enhanced Raman spectroscopic enhancements. This has also been the topic of multiple reviews, as well as a recent past Faraday Discussion.[22-28] The near-field enhancements of plasmonic structures have also been shown to benefit device properties, in particular, enhancing photovoltaic efficiencies.[29-32] While the focus of this field on hot electron science has been a more recent development,[33,34] in many ways it has the potential to eclipse earlier advancements in importance. Because there are already several useful and comprehensive reviews on hot carriers in plasmonics,[35,36] in this introductory article, we will focus specifically on two topics within hot electron science: hot electron photodetection, and hot electron photocatalysis. Our introduction begins with a theoretical analysis of hot carrier generation in metallic nanoparticles induced by plasmon decay.[37] Here, through a straightforward theoretical model, we examine some of the essential dependencies of hot carrier generation, such as the dependence of hot carrier generation rate and the energies of the hot carriers produced on the absorption spectrum of a particle, particle size and carrier lifetime. We then turn to hot electron-based photodetection, a mechanism that drives a subset of the growing number of plasmonic photodetection devices of various types.[38] Hot electron-based photodetection brings new light-detection mechanisms to photocurrent-based photodetector devices, making it possible to detect light below the semiconductor bandgap.[39,40] The combination of plasmonics and electronic photodetection allows for spectral and polarization selectivity in light detection, which offers the opportunity to design specialized photodetection strategies that would by conventional approaches be far more complex.[39,41] Hot electron-based photodetection can also provide insight into the properties of the hot carrier generation process itself, providing clues to how enhancing this process could result in higher-performance photodetectors.[42] On the topic of plasmon-based photodetection, extending device designs to new materials such as graphene creates new benchmarks for photodetector device performance.[31,43] Hot-carrier photocatalysis provides new approaches to the design of catalysts for chemical reactions, and offers new possibilities for converting thermally-driven catalytic processes into light-driven processes that require substantially lower operating temperatures. We also discuss the importance of incorporating new materials, in particular, catalytic metals whose surface reactivities but poor optical absorptive properties complement those of noble/coinage metals alone, and how plasmonic and catalytic metals can be combined into "antenna-reactor" complexes. Finally, since the nonradiative decay of a surface plasmon results in both hot electron generation and photothermal heating, we discuss how to clearly distinguish between the two processes in plasmonic photocatalytic reactions.

Properties of plasmon-induced hot carriers in metal nanoparticles

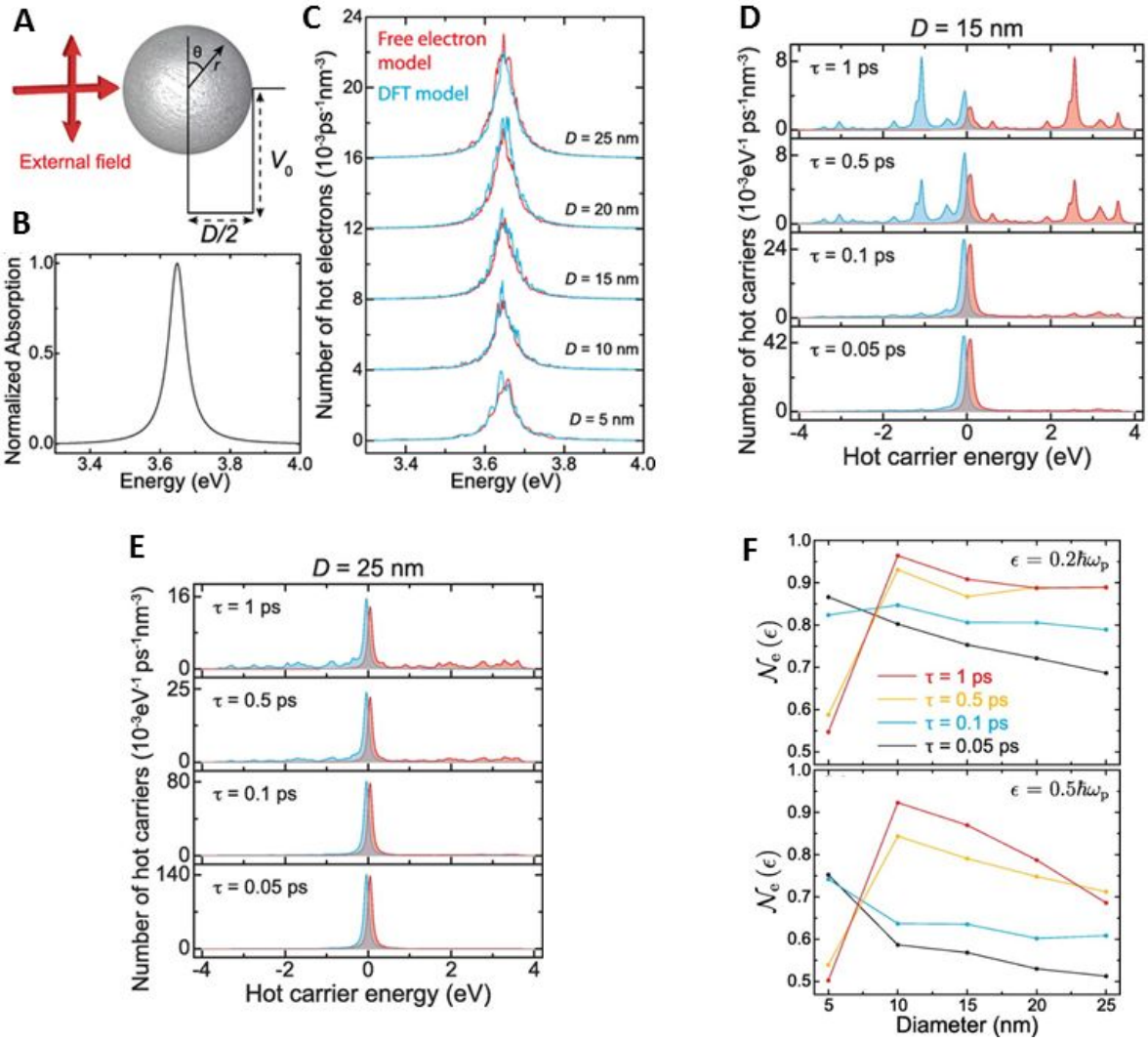

Figure 1.(A) Schematic of theoretical model for plasmon-induced hot carrier generation. (B) Calculated optical absorption of Ag nanoparticle. (C) Number of hot electrons generated per unit time and volume as a function of wavelength. (D) Hot carrier number and energy distribution for a resonantly illuminated Ag nanoparticle with diameter of 15 nm, for carrier lifetimes ranging from 0.05 to 1 psec. Red: electrons; Blue: holes. (E) hot carrier number and energy distribution for a resonantly illuminated Ag nanoparticle with diameter = 25 nm, for the same range of carrier lifetimes as in (D). (F) The efficiency of hot electron generation due to resonant illumination of an Ag nanoparticle, as a function of particle diameter and carrier lifetime. The decrease in hot electron generation efficiency which is clearly indicated for both increasing particle diameter and decreasing carrier lifetime is clearly reversed for nanoparticle diameters in the 5 nm range. From Reference 37.

By applying a straightforward theoretical model, Manjavacas and Nordlander have elucidated several essential characteristics of hot carriers resulting from plasmon-resonant excitation of a metal nanoparticle.[37] Their model describes a spherical Ag nanoparticle with a diameter ranging from 5 to 25

nm (quasistatic limit) as free carriers in a finite spherical potential well, considering only the conduction electrons (Fig. 1A). External illumination results in the excitation of a plasmon, described as a classical field. Hot carriers are generated by the action of the external and the plasmon-induced electric fields, which act upon the conduction electrons, inducing transitions from initial states below the Fermi level to final states above it. The probability of hot electron generation is calculated using Fermi's golden rule. Within this picture, the particle size and the carrier lifetimes are both varied to better understand hot carrier properties. Carrier lifetimes (not to be confused with plasmon lifetimes of ~10 fsec) are limited by electron-electron, electron-surface, and electron-phonon scattering, and range between $0.05 < \tau < 1$ psec. Although this model does not capture the fully quantum nature of the plasmon response of the metal, [44] several important aspects of hot electron generation rates and energies are well described with this model. First, the number of hot electrons generated by illumination per unit time and volume as a function of wavelength established that hot electron generation directly follows the absorption spectrum of the nanoparticle (Fig. 1B, C). This means that direct excitation of hot electron-hole pairs, which is present also for nonresonant excitation, is a many orders of magnitude less efficient process for hot carrier generation than plasmon decay. This result was also compared directly with equivalent calculations performed using density functional theory (DFT) (Fig. 1C). The striking similarity of the two theoretical approaches verified that this model was useful for the regime being studied, and also that many-body effects such as exchange-correlation have only a minor impact on hot carrier generation in the regime considered (high plasmon quantum number; classical excitation) and can be neglected. The energy distribution of hot electrons and holes was then calculated for a range of carrier lifetimes and nanoparticle diameters (Fig. 1D, E). This calculation contains several striking results. It is clearly apparent that the carrier lifetime has a direct influence on the energy of the hot carriers that can be generated by illumination (this model applies to illumination times much longer than the carrier lifetimes). Short carrier lifetimes result in higher number but lower energy, "cooler" hot carriers. The particle diameter has a similar influence, with smaller nanoparticles yielding more energetic carriers, a result that reflects several experimental plasmonic photocatalysis studies where smaller nanoparticles appeared to more efficiently generate transient negative ion states of adsorbate molecules than larger nanoparticles.[45] However, when we look at the total generation rate independent of energy distribution, we find that it is largest for larger nanoparticles and shorter carrier lifetimes (Figs. 1D and E, y axes). A hot carrier generation efficiency was also defined as the number of hot electrons generated per excited plasmon that have an energy larger than a certain threshold (Figs. 1F) . This generation efficiency was calculated as a function of nanoparticle diameter, for the range of hot carrier lifetimes being considered. Here we see that the hot carrier generation efficiency decreases with increasing nanoparticle diameter for sizes 10 nm and larger, and also decreases with shorter carrier lifetimes. For nanoparticles smaller than 10 nm, these trends do not hold, most likely because of the discrete nature of the energy levels that begins to become apparent for this smaller size regime.

While this study yields insight into the properties of plasmon-induced hot electrons, the essential point of this analysis is that ***the time-dependent E field within the nanoparticle during plasmon-resonant optical excitation is directly responsible for hot carrier generation.*** This is the essential starting point for the design of effective structures and devices that use hot electrons for various applications. This is a unique aspect of plasmonic behavior that differs from the properties of bulk metals, since bulk metals screen external fields extremely well. In the sections that follow, we will examine the importance of this property in two applications: hot electron-based photodetection and hot carrier plasmonic photocatalysis.

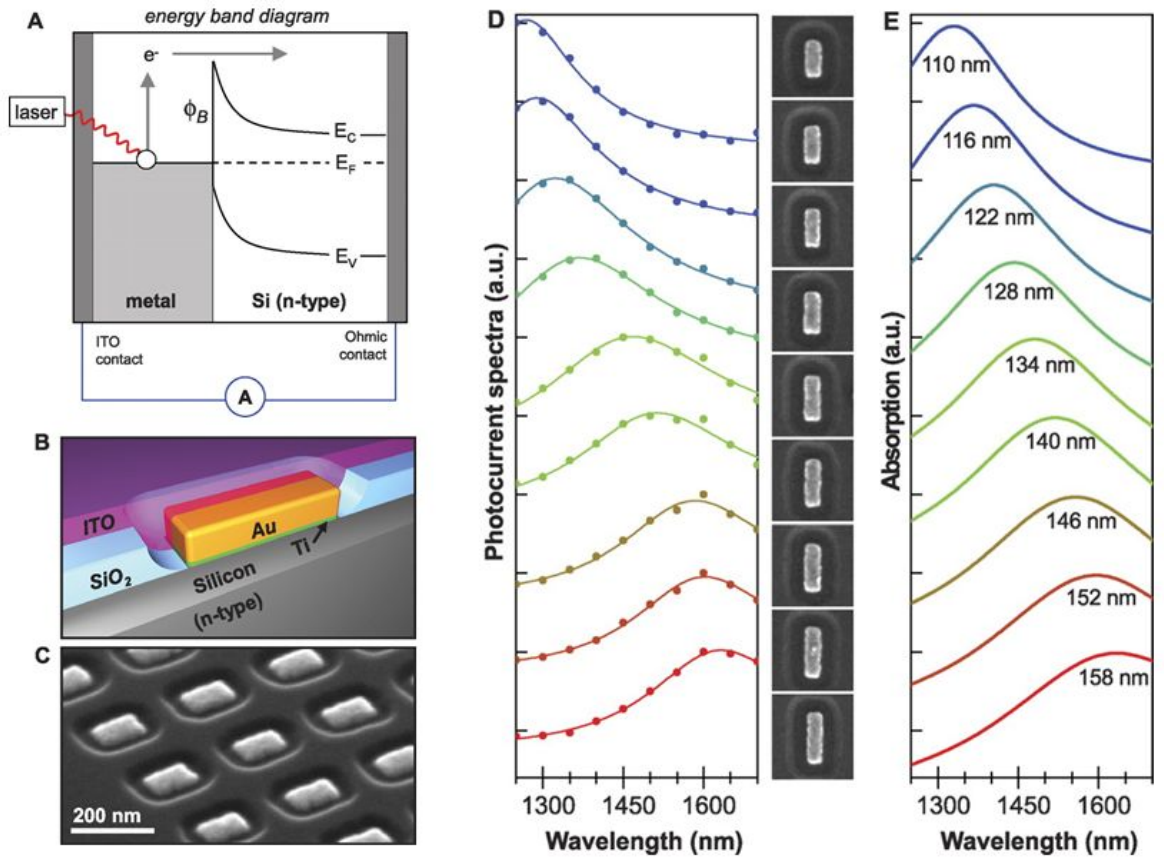

Figure 2. (A) Band diagram for plasmonically driven internal photoemission over a nanoantenna-semiconductor Schottky barrier (fB). (B) Representation of a single Au resonant antenna on an n-type silicon substrate. (C) Scanning electron micrograph of a representative device array prior to ITO coating, imaged at a 65° tilt angle. (D) Photocurrent spectra of nine devices with arrays of nanorods of various lengths (shown). (E) Corresponding calculated absorption spectra. From Reference 39.

Hot electron-based photodetection

A hot electron-based photodetector is created when a plasmonic structure is on a semiconductor such that a Schottky barrier is formed at the interface (Fig. 2A).[39,40] When the plasmon energy is larger than the Schottky barrier height, hot electrons are injected into the conduction band of the semiconductor. The plasmonic nanostructures must be electrically connected to avoid charging and to complete the electrical circuit, which in this case is accomplished by covering the front face of the active area of the device with a conductive transparent oxide (indium tin oxide, ITO) layer (Fig. 2B). The initial device consisted of a square array of nanorods of equivalent length (Fig. 2C) patterned by e-beam lithography onto an n-type silicon substrate with a titanium adhesion layer, followed by deposition of the ITO layer. The device can be operated without a bias voltage, although applying a bias voltage greatly improves its responsivity. There are several interesting and unique properties of this type of photodetector. First, this photocurrent generation mechanism is not limited by the bandgap of the semiconductor, enabling photocurrent generation at longer wavelengths, where the photon energy is

insufficient to create electron-hole pairs in the semiconductor itself (Fig. 2D). Second, the resonance of the plasmonic nanostructure used for hot carrier generation defines the spectral response of the photodetector. Therefore this type of photocurrent generation mechanism is inherently spectrally selective, which enables the possibility of hot electron photodetector arrays of various resonances serving as a fully integrated spectrometer-detector. For plasmonic nanostructures with polarization sensitivity, this characteristic as well is imparted onto the photodetector. By systematically modifying the aspect ratio of the nanorod components of the array, the spectral response of the detector can be tuned (Fig. 2D). As mentioned in the earlier theoretical discussion on the spectral response of hot electron generation, we see that the photocurrent spectral response here follows the optical absorption of the nanorod arrays used in each device (Fig. 2E).

By modifying photodetector device design, one can directly investigate and quantitatively compare the properties of hot electrons induced by plasmon excitation relative to those induced by absorption in the metal itself.[42] As we saw in the theoretical study discussed earlier, hot carrier generation is dependent upon the E-field inside the metal, strongly enhanced when illuminated on resonance. Generally, it is localized to regions of large field enhancements on more complex structures. Hot carriers can also be generated due to light absorption in the metal, limited by its optical absorption depth at that wavelength. In Au, carrier generation by direct photoexcitation results from the excitation of d-band electrons into the conduction band.

In Figure 3 we show a hot-electron photodetector that consists of an Au grating that extends from an Au film. The grating structure is fabricated onto a TiO_2 substrate, a wide bandgap n-type semiconductor. The wide bandgap of the semiconductor allows preferential collection of electrons. Surface plasmons are launched by illumination onto the grating structure[41] (their resonant wavelength is ~675 nm); the film "pad" allows for good electrical continuity between the plasmonic grating structure and the semiconductor substrate. When the Au grating structure is fabricated directly onto TiO_2, it forms a Schottky barrier measured to be, on average, 1.07 eV (Fig. 3A). This compares quite well with the literature value of 1 eV. When an intervening Ti layer is deposited on the TiO_2 prior to Au deposition and fabrication, the barrier is Ohmic instead (Fig. 3B). The band diagrams for the Schottky and Ohmic devices are shown in Figures 3C and 3D, respectively. For the Schottky device, the photocurrent must be due to hot electrons, while all photocurrent generated will be detectable in the Ohmic device. Resonant illumination of the grating for TE polarization (Fig. 3E) results in plasmon excitation. By scanning the device and measuring the photocurrent response, a photocurrent map is created (Fig. 3F for the Schottky case and Fig. 3G for the Ohmic case). This map indicates from what location on the device structure the detected photocurrent originates. For the case of plasmon excitation, we observe that there is a relatively strong photocurrent signal originating from the region of the grating structure, for both the Schottky and the Ohmic cases (Figs. 3F, G). By rotating the polarization of the incident light (Fig. 3H), plasmons are not excited on the grating structure. In this case, the photocurrent maps show that the photocurrent, substantially less for both the Schottky and the Ohmic devices, originates in different regions of the device. For the Schottky case, virtually no photocurrent is observed for illumination either of the grating or the Au film, with only a minor response observed on the edges of the structure where the film meets the grating. For the Ohmic case, the observed photocurrent originates primarily on the Au film, with a smaller contribution from the grating structure. These data show that plasmon excitation results in much hotter electrons (Fig. 3F) than non-plasmonic direct excitation of carriers, with the latter excitation mechanism resulting in virtually no electrons with sufficient energy to traverse the Schottky barrier (Fig. 3I). In the

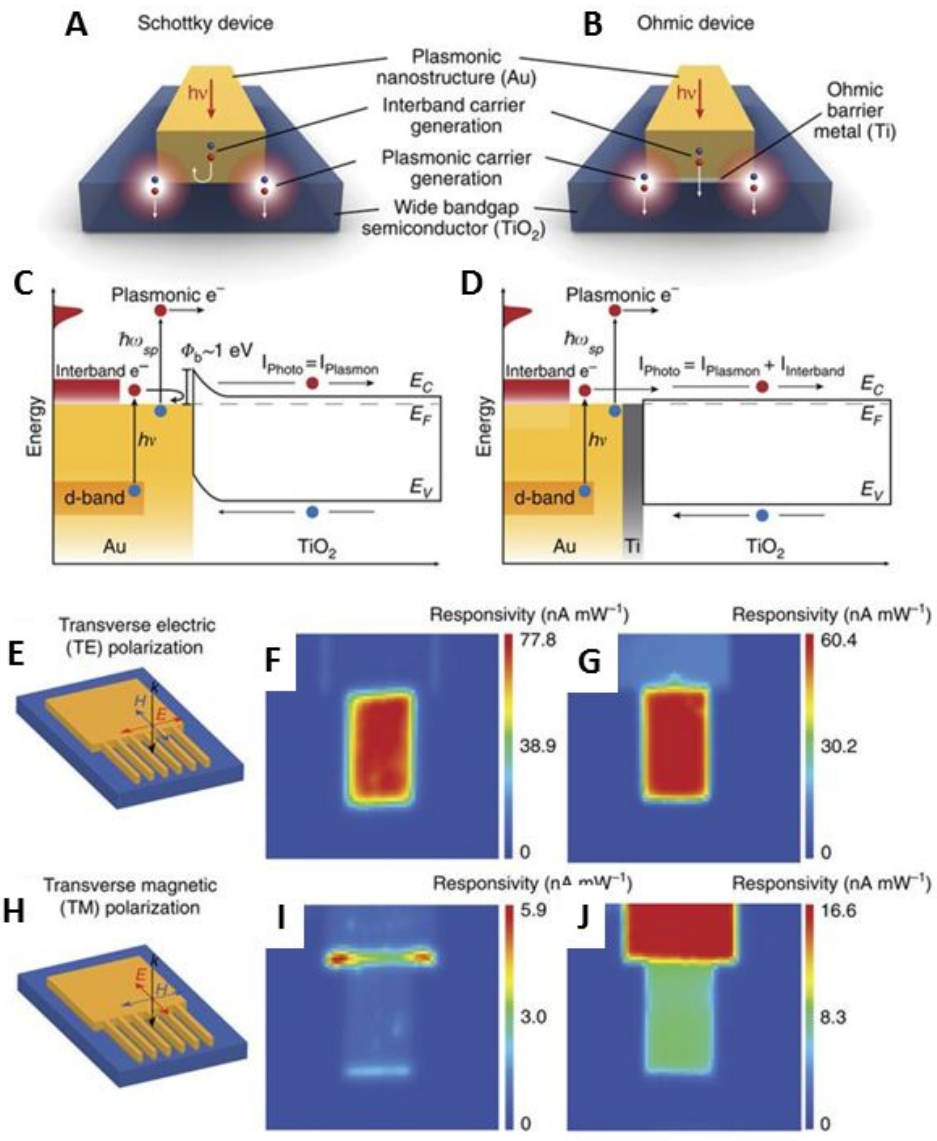

Figure 3. Schematic of hot-carrier generation and collection over a Schottky (A) or an Ohmic barrier (B). Band diagram schematics of (C) a Au-TiO_2 Schottky device and (D) a Au-Ti-TiO_2 Ohmic device. (D-J) Photocurrent mapping. (E) Schematic of TE excitations used to generate photocurrent maps. The laser wavelength is tuned to the resonance of the plasmonic nanowires. Photocurrent maps of a (F) Schottky and (G) an Ohmic device using TE-polarized light. (H) Schematic of TM- polarized light excitation. Photocurrent maps of a (I) Schottky and (J) an Ohmic device. From Reference 42.

Ohmic, barrierless case, we can see that plasmon excitation of the grating gives rise to more than seven times as many carriers in the grating itself (Fig. 3G) than in the case where optical absorption is the only mechanism for photocurrent generation (Fig. 3J). Theoretical analysis of the photocurrent response of this detector shows explicitly that the photocurrent in the Schottky case depends only on the near-field inside the metal generated by plasmon excitation, while the photocurrent in the Ohmic case depends on both the inherent material absorption as well as the plasmonic near-field induced by plasmon excitation.[42]

This device provides clear evidence of what was shown theoretically, [37] that the internal near-field generated by plasmon excitation is the quantity that determines hot carrier generation.

Since initial demonstrations, hot-carrier photodetectors have been demonstrated using 2D materials such as MoS_2, graphene,[12] and other materials as the current collector. Greater sophistication in the development of plasmonic antennas with Fano resonances[46], [43] and perfect absorber geometries[38] have also been implemented to increase device responsivities. Combining these effects with other current-enhancing properties in semiconductors, most notably free-carrier absorption, has also been demonstrated.[47] Further developments of hot electron-based photodetectors should ultimately lead to performance comparable to current commercial systems, which should result in new spectrally sensitive detection capabilities in compact lightweight device geometries.

Plasmon-induced hot electron-based photocatalysis

Emerging primarily from earlier studies of femtochemistry on well-defined index faces of metallic crystals, the transition to metallic nanoparticle-based photocatalysis enabled the direct optical excitation of nanoparticle plasmons, substantially boosting hot electron generation. The transition from index face

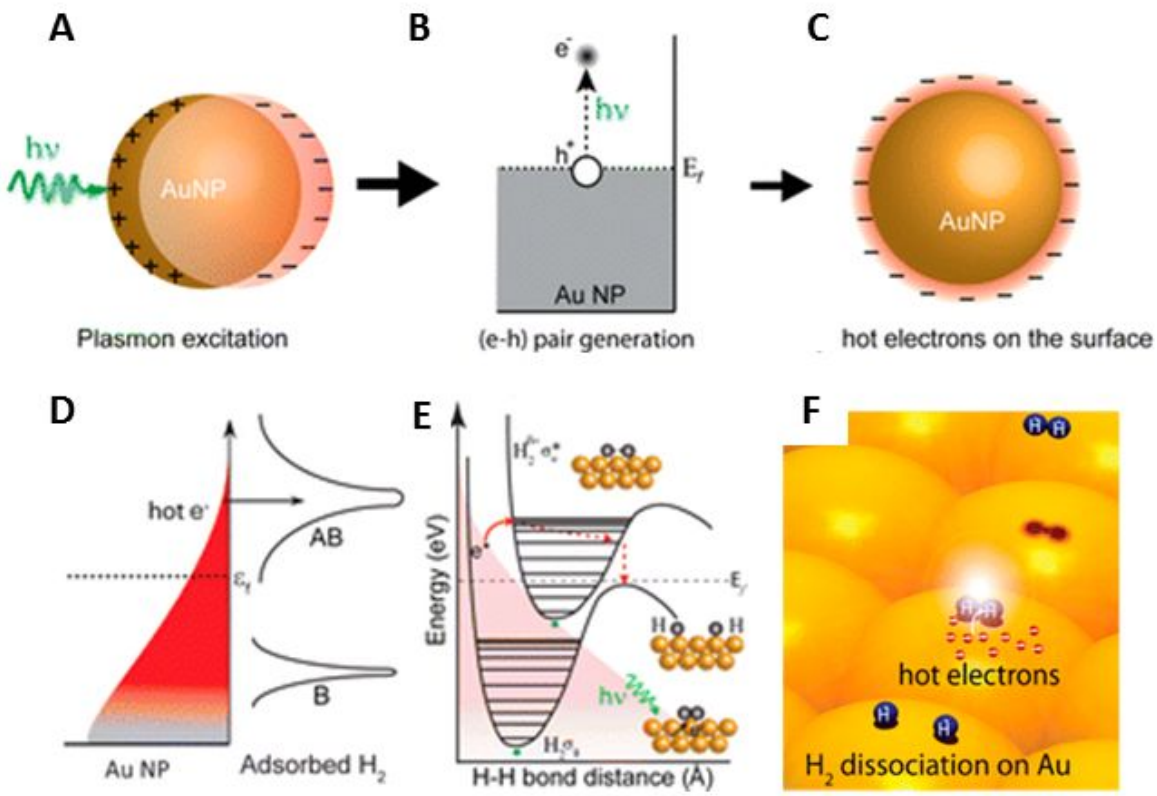

Figure 4. (A) Schematic of plasmon excitation, (B) e-h pair generation, and (C) hot electrons available at the nanoparticle surface. (D) Schematic of Fermi–Dirac distribution of hot electrons permitting hot electron transfer into the antibonding state of H_2. (E) Proposed mechanism of hot-electron induced dissociation of H_2 at the Au nanoparticle surface. (F) Schematic of H_2 dissociation mediated by hot electron transfer and formation of transient negative ion state, $H_2^{-\delta}$ followed by dissociation. From Reference 45.

studies using high-power lasers to studies of metal nanoparticles was motivated by the desire to develop photocatalysts for reactions that are of direct industrial interest. The chemical industry is one of the highest consumers of energy worldwide, and lowering this energy consumption level has long been a primary motivating factor for catalyst development. On metallic nanoparticles, processes that are driven by hot electrons can dominate surface chemistry, change reaction outcomes relative to thermal processes, and lower reaction barriers such that reactions can proceed at substantially lower temperatures than under conventional conditions.[48] Pioneering work in the area of hot electron photocatalysis includes liquid phase water splitting,[49-51] H_2 production from alcohol,[52,53] gas phase oxidation reactions,[54,55] and hydrocarbon conversion.[56]

In plasmonic photocatalysis, plasmon excitation leads to hot electron-hole pairs: the hot electron cloud extends from the nanoparticle surface due to the shape of the surface potential (Figs. 4 A-C).[45] For the case of plasmonic H_2 dissociation illustrated here, if an H_2 molecule is present, the electron can transfer from the metal to the LUMO level of the adsorbed species on or near the metal surface, creating a transient negative ion, $H_2^{-\delta}$ (Fig. 4D, E). In general, the detailed nature of this charge transfer process in specific systems has been studied and debated in the literature. However, its role as an important mechanism in plasmonic photocatalysis is widely accepted. The additional Coulomb repulsion in the molecule increases the H-H bond distance and lowers the barrier to dissociation relative to the case of the neutral molecule (Fig. 4E). Calculations on an isolated hydrogen molecule show that H_2^- has a metastable state located about 1.7 eV above the ground state of the neutral molecule.[45,57] The bond dissociation energy for this state is 2 eV lower than for the neutral case (2.6 eV vs. 4.6 eV). The process occurs at room temperature with visible light at a wavelength that corresponds to excitation of the localized surface plasmon of the nanoparticle.

The experimental system for H_2 dissociation is shown in Figure 5. Very small Au nanoparticles were dispersed in an oxide matrix (TiO_2). The size dependence of the Au nanoparticles proved to be quite important, and for nanoparticles larger than 10 nm in diameter the photocatalytic activity was reduced relative to the smaller nanoparticles. Smaller size Au nanoparticles likely have slower electron thermalization rates due to reduced electron-phonon interactions. The role of the TiO_2 matrix is to reduce the diffusion of the gas molecules on the surface of the Au, and does not directly participate in the reaction. It was discovered subsequently, by performing the same experiment using an SiO_2 matrix, that TiO_2 can actually compete as an electron scavenger with the H_2 adsorbate molecules. [57] H_2 dissociation is detected by using both H_2 and D_2 reactants and looking for the presence of HD using a mass spectrometer (Fig. 5C). The HD signal corresponds to illumination of the plasmonic photocatalyst (Fig. 5D). The small amount of photothermal heating, roughly 5-6 degrees Celsius, does not contribute significantly to HD formation (Fig. 5E). This very simple chemical reaction with no side products can serve as a benchmark for plasmonic photocatalyst design, and allows us to learn in greater detail about the role of the metal nanoparticle in mediating hot electron processes. For example, the same experiment was performed on Aluminum nanocrystals (Al NCs), which were found to be photocatalytically reactive relative to Au nanoparticles for the case of H_2 dissociation.[58] Here Al was chosen as the plasmonic metal because it is the most earth-abundant plasmonic metal, and also because of its highly attractive properties in nanostructure form.[59] In the case of Al NCs acting as the plasmonic photocatalyst for H_2 dissociation, charge transfer was already found to be substantial for ground state H_2, suggesting that the electron affinity level of the H_2 molecule lies very close to the Fermi level of the Al NC. Because the affinity level is close to the Al Fermi level, it overlaps the photo-induced hot electron distribution. The reaction barrier

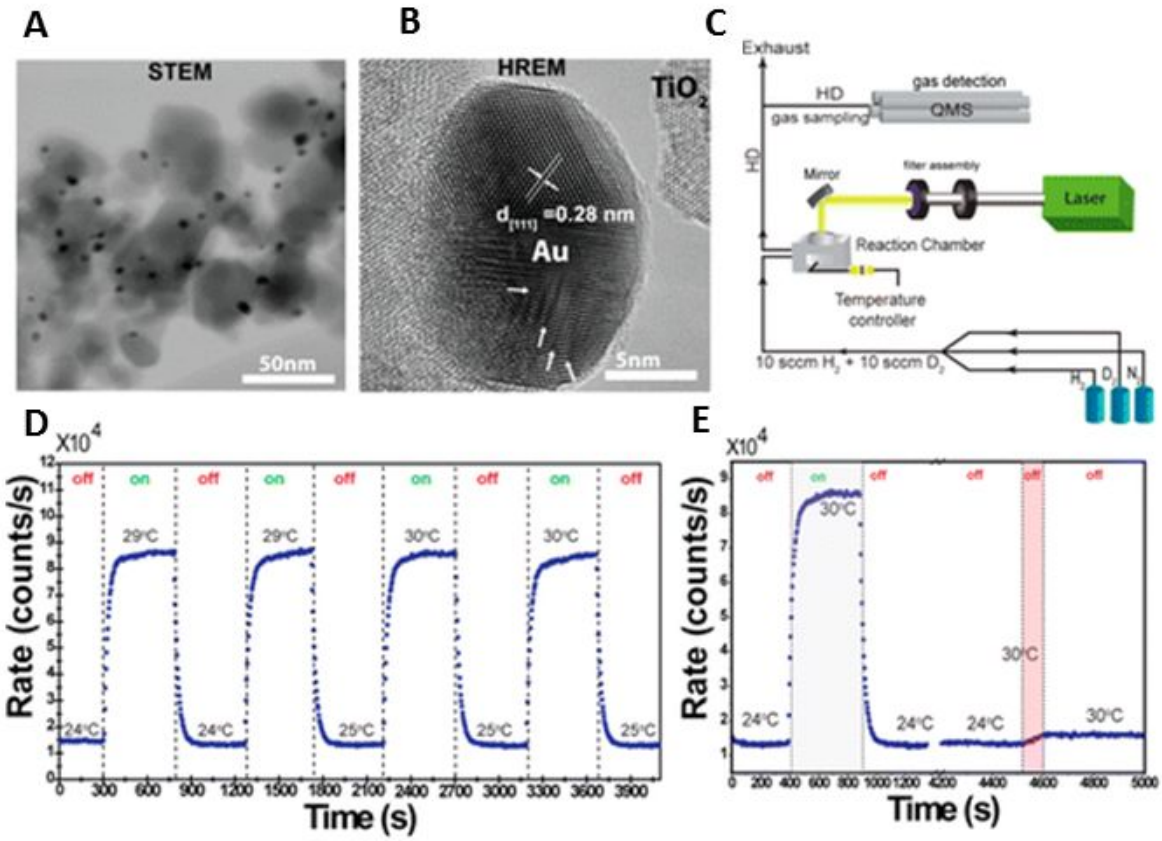

Figure 5. Plasmon-induced dissociation of H_2/D_2 using 1.75 wt % Au/TiO2 photocatalyst at room temperature (297 K). (a) Scanning transmission electron micrograph showing distribution of 1.75 wt % AuNPs (dark particles) over a TiO_2 support (gray). (b) High-resolution transmission electron micrograph of a single Au NP supported on TiO_2 matrix showing darker contrast of Au NP as compared to TiO2 support. Characteristic lattice fringes of Au (111) and (200) are visible at ~2.8 Å and 2.3 Å, respectively. (c) Schematic of overall experimental setup. (d) Real time monitoring of rate with laser excitation (on 2.41 W/cm2) and without laser excitation (off). During 8 min of laser irradiation on the photocatalyst, the temperature increases by 5 K as shown in the figure, from 297 to 303 K. The dotted vertical lines indicate the laser on/off times. (e) Distinction between the photocatalytic rate (only laser on, 2.41 W/cm2) and thermal heating rate (laser off, heating on). The shaded gray area displays the photocatalytic rate due to the laser. The shaded red area displays the rate of HD formation due to heating of the photocatalyst sample from room temperature (297 K) to 303 K without laser illumination. From Reference 45.

for hydrogen dissociation is further lowered after injection of a hot electron from the Al nanoparticle into the antibonding orbital. For Al, the energy of maximum HD generation corresponds to its interband transition, not its plasmon resonance.

Antenna-Reactor Hybrid Nanoparticles for Hot-electron Photocatalysis

Plasmon-based photocatalysis was initially demonstrated with noble/coinage metals, with their strong plasmon-derived optical near field and resultant hot carrier generation. Conventional

heterogeneous catalysis has developed using weakly light-absorbing metals such as Pd, Pt, Ru, or Rh to lower the activation energy for chemical reactions under conditions that typically require high temperatures and pressures. Combining the optical properties of plasmonic metals with the chemical reactivities of catalytic ones would open the door to new types of photocatalytic processes, essentially converting catalysts into photocatalysts. This can be accomplished by developing hybrid systems where a plasmonic nanoparticle acts as an "antenna" for a nearby catalytic "reactor" nanoparticle. Other variations of this concept, such as reactive surface alloys on a plasmonic nanoparticle, can be developed based on the same principle.

The initial realization of the antenna-reactor principle is shown in Figure 6(A).[60] The idea is based on the concept originally discussed in Figure 1: that the photoexcited plasmon decays by generating hot electrons. Here, the plasmon mode of the antenna itself is photoexcited, and if the reactor nanoparticle is within the antenna particle's near field, it will also be photoexcited even though it may have no inherent optical absorption itself at the plasmon-resonant wavelength of the antenna particle. It is important to realize that this photoexcitation of the reactor particle by the antenna particle does not require the two to be conductively coupled: there need be no charge transfer between the antenna and reactor nanoparticles. In fact, if the two particles were in conductive contact with each other, the reactor would likely dampen the plasmon resonance of the antenna particle. The case illustrated in Figure 6(A) involves two nanoparticles deposited adjacent to each other on a planar substrate, for example, where the only (nonmechanical) coupling between the two nanoparticles is through the antenna particle's fringing field. Physically, the fringing field of the antenna particle induces a similar electron oscillation in the reactor particle as in the antenna particle itself: we can think of this as a "forced plasmon" in the reactor driven solely by the antenna particle under photoexcitation. In contrast to direct excitation of hot electron hole pairs which is a single-particle excitation process, this forced plasmon is a collective but strongly damped excitation which only can decay nonradiatively. Just as the plasmon mode of the antenna particle decays by the generation of electron-hole pairs, the same process should occur in the "forced plasmon" of the reactor particle. In Figure 6(B), the geometry of an Al nanoantenna particle (approximated as a sphere), with a 2-4 nm thick native oxide coating, on with a Pd hemispherical reactor particle is deposited, is shown.

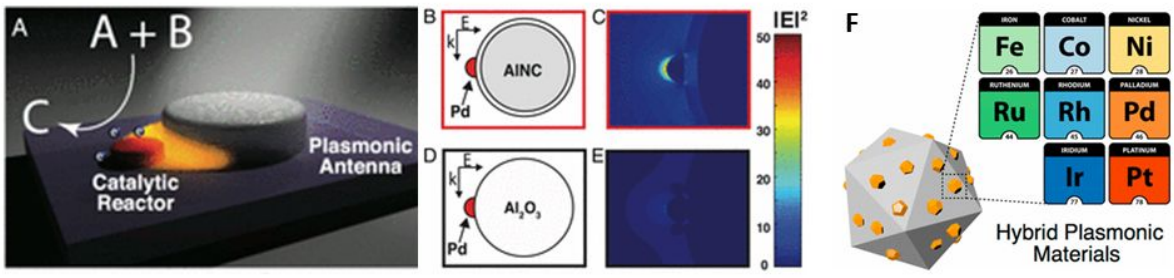

Figure 6. (A). The antenna-reactor concept, which shows a plasmonic nanoparticle being illuminated and the near-field being generated, with the catalytic reactor nanoparticle located within the fringing field of the antenna nanoparticle. (B) a prototype antenna-reactor is illustrated consisting of an Aluminum nanocrystal antenna with a small Pd reactor nanoparticle (C) the local field enhancement of (B) shows a strong field on the Pd surface at the resonant plasmon wavelength of the Al NC. (D) for a Pd reactor on an Aluminum oxide nanoparticle, no light absorption, and therefore no near field at the Pd surface, is visible. (F) the modularity of the antenna-reactor concept is illustrated, where a range of different type of catalytic reactor nanoparticles can be adsorbed onto the Al NC surface for enhancing specific reaction rates and outcomes. From Ref. 60 (A-E) and Ref. 61(F).

Under resonant illumination of the antenna particle, the local $|E|^2$ at the reactor particle surface is calculated (Fig. 6(C)). This geometry is compared to the case of a Pd hemispherical reactor particle deposited instead on a nanosphere consisting entirely of Al_2O_3: in this case there is no field enhancement at the Pd surface (Figs. 6D, E). A schematic illustration of the spherical antenna-reactor geometry as envisioned as a modular photocatalyst design is depicted in Figure 6F. Here, the Al NC antenna, whose plasmon mode can be tuned in energy by varying the particle size, can be decorated by a variety of different catalytic metals as reactor particles.[61]

In light of our previous discussion regarding H_2 dissociation on plasmonic Au and Al antenna particles, it is interesting to see how this reaction proceeds on an antenna-reactor particle. As illustrated in Figure 6, the Al NC antenna-Pd reactor particle was both chemically synthesized[60] and also fabricated using a planar plasmonic heterodimer geometry. [62] A head-to-head comparison of H_2 dissociation on pristine Al NC nanoparticles and chemically synthesized Al NC-Pd antenna-reactor particles is shown in Figure 7. The wavelength dependence (Fig. 7(A)) clearly indicates that the reaction proceeds differently on the two different plasmonic photocatalysts. What is not indicated in Fig. 7(A) is that the HD yield for the antenna-reactor particles is almost two orders of magnitude higher than for the pristine Al NCs.[60] For the antenna-reactor complex, the maximum reactivity occurs when the dipolar plasmon of the antenna particle is excited, in stark contract to the pristine Al NC case, where maximum reactivity occurs at wavelengths consistent with the interband transition of Al. From these data it is clear that the reaction pathways on the two photocatalysts are very different. It is well established that dissociative adsorption of H_2 occurs in an essentially barrierless manner on Pd.[63,64] In contrast to the hot electron transfer process for H_2 dissociation on pristine Au and Al nanoparticle surfaces, here the hot electrons generated in the Pd by forced plasmon decay are responsible for inducing desorption of H and D, which quickly recombine. This is a charge neutral process: once the chemical reaction is completed, the hot electrons recombine with the holes in the Pd islands. It is also evident in Fig. 7(A) that the HD production on Al NC-Pd antenna-reactor nanoparticles follows the optical absorption of the nanoparticle complex very closely, in agreement with our earlier-discussed theoretical analysis of hot electron generation in plasmonic nanoparticles (Fig. 1B, C). In Figure 7(B) the laser power dependence of the HD generation rate is shown for the two wavelengths corresponding to the dipolar antenna-reactor plasmon mode and the interband

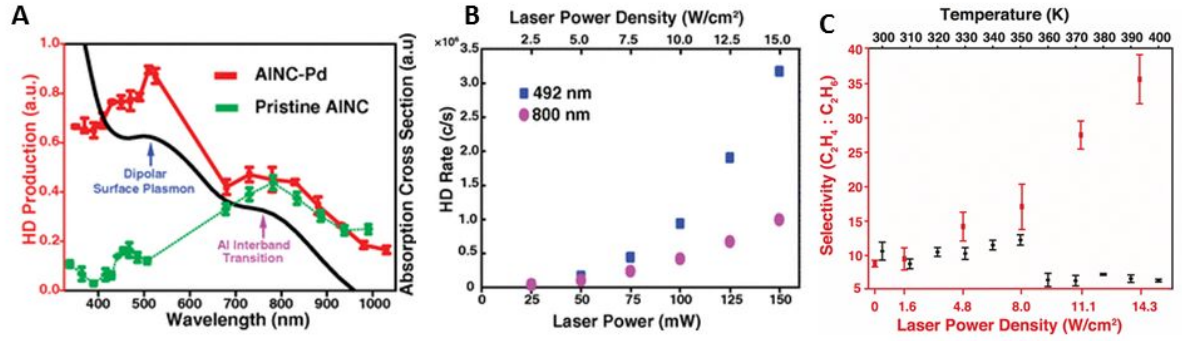

Figure 7. (A) The wavelength dependence of the H_2 photocatalytic dissociation reaction performed using Al NCs (green) and Al NC-Pd antenna-reactor complexes (red). (B) power dependence of H2 dissociation on Al-Pd antenna-reactor particles. (C) Acetylene hydrogenation reaction on Al NC-Pd antenna-reactor particles: here we examine the ethylene/ethane selectivity, comparing the photocatalyzed reaction (red) and the thermally catalyzed reaction (same complexes, reaction run thermally with no photoexcitation, black). From Reference 60.

transition at 800 nm, respectively. The supralinear power dependence observed here is consistent with other hot electron-induced photocatalytic processes.[65]

In addition to studying the H_2 dissociation reaction on Al-Pd antenna-reactor particles, the hydrogenation of acetylene was studied, comparing the photocatalytic reaction to the thermocatalytic reaction on the same antenna-reactor complex (Fig. 7(C)). In this reaction, which is quite important industrially, both ethylene and ethane are the reaction products, and ethylene selectivity is highly desired. What is observed is a high selectivity of the photocatalytic process to ethylene synthesis relative to the thermal process. Ethylene/ethane ratios as high as 37:1 were observed for the photocatalysis case, where for the thermal case ethylene/ethane ratios never increased above 10:1. It has been postulated that the selectivity enhancement of photohydrogenation is likely due to the availability of dissociated H_2 in this case, again, induced by hot electron desorption on the reactor nanoparticles. In a theoretical analysis it was found that the Pd-H antibonding interactions were energetically just above the Fermi level, easily populated by hot electrons. Therefore a hot-electron-initiated destabilization of the Pd-H bond, leading to desorption, is a plausible mechanism. The facile hot-electron-induced desorption of H_2 from the surface

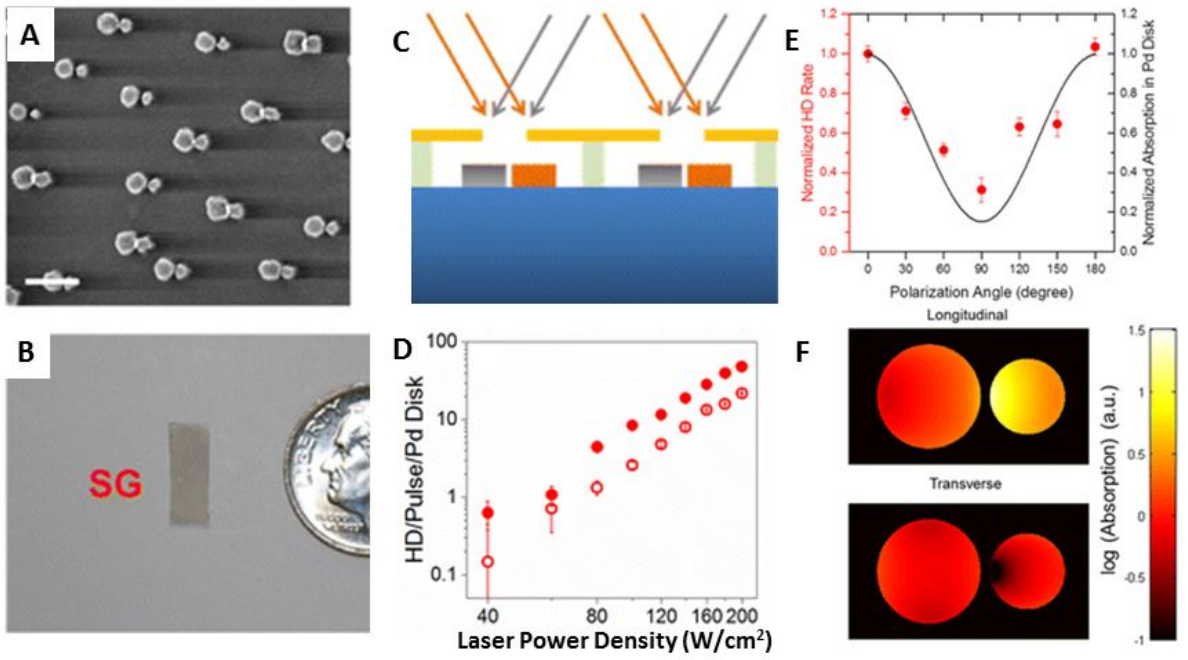

Figure 8. (A) Scanning Electron Microscope (SEM) image of a sample of Al-Pd heterodimers, fabricated over a large area (B) suitable for photocatalysis. A fabrication method known as hole-mask lithography (C) was used to fabricate heterodimers with precisely defined nanogaps over such a large area. (D) by performing the H_2 dissociation reaction on a fabricated substrate where the density of antenna-reactors is known, the production rate of # HD molecules per laser pulse per antenna-reactor structure was determined as a function of incident laser power density (W/cm^2). (E) the Al-Pd heterodimers also showed a polarization sensitivity to their photocatalytic response. (F) theoretical analysis using the finite-difference time-domain method shows the absorption induced by the Al nanodisk on the Pd nanodisk for longitudinal (top) and transverse (bottom) incident light polarization. From Reference 62.

limits the hydrogenation of acetylene, promoting ethylene over ethane as the reaction product.

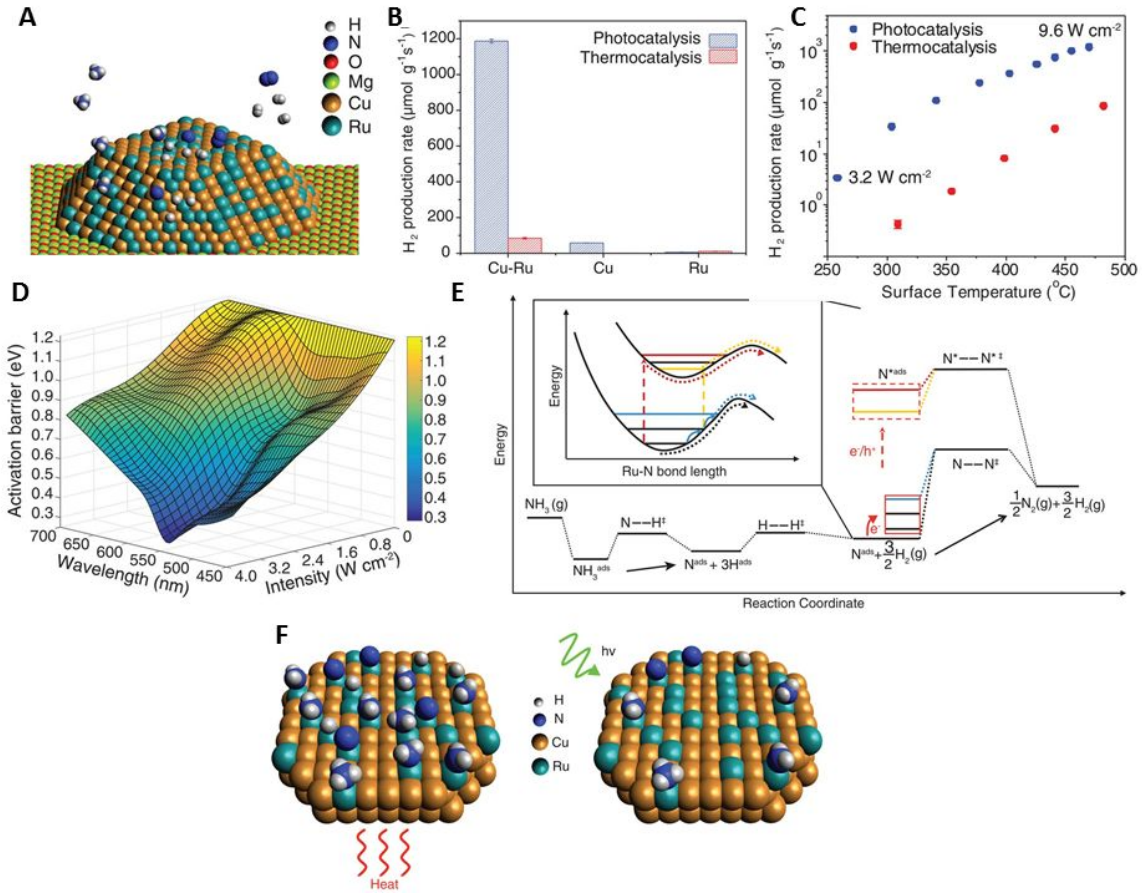

Figure 9. (A) Schematic of the Cu-Ru antenna-reactor photocatalyst, on its MgO support. (B) the photocatalytic behavior of the antenna-reactor towards ammonia decomposition was found to be far greater than its thermocatalytic activity, which in turn was found to be more active than either a pristine Cu or Ru nanoparticle. (C) both the photocatalysis and thermocatalysis reaction rates increased with increasing surface temperature. (D) Arrhenius plots of the apparent reaction barriers for illumination wavelengths and surface temperatures (controlled with temperature controller) were measured for a range of illumination conditions, varying both laser power and wavelength. From this data, a light-dependent decrease in reaction barrier can be defined, where the reaction barrier in the dark (1.2 eV, right axis) is reduced as a function of both wavelength and light intensity, to a value as low as 0.2 eV at 550 nm illumination wavelength. (E) this reduction in activation barrier changes the rate-limiting step of the reaction, from associative desorption of N_2 to the N-H bond breaking step. (F) the physical mechanism for the change in rate-limiting step is the hot electron-induced desorption of N_2 from the Ru reactive sites (right), freeing those sites for further adsorption and decomposition of NH_3 adsorbate molecules. The lack of a desorption mechanism in the thermal case (left) makes N_2 desorption the rate-limiting step. From Reference 68.

To additionally demonstrate the antenna-reactor photocatalysis concept (Fig. 6(A)), a large-area sample

of Al-Pd plasmonic heterodimers was fabricated (Fig. 8) using the method of hole-mask lithography (Fig. 8(A-C)). The heterodimers were photocatalytically active, and since their density on the sample surface was known, the number of HD molecules produced per laser pulse, per photocatalytic antenna-reactor, could be determined as a function of incident laser intensity (Fig. 8(D)). As plasmonic heterodimers, the fabricated structures with well-defined gaps showed a polarization dependence for their photocatalytic activity (Fig. 8(E)), consistent with the near-field enhancement induced in the Pd reactor disk of the heterodimer, which varied strongly as a function of polarization angle (Fig. 8(F)). These types of nanofabricated antenna-reactors may be useful for antenna and reactor material combinations that are difficult to fabricate using chemical synthesis approaches.

Quantifying hot electron and thermal contributions to plasmonic photocatalysis

It is important to remember that the resonant illumination of a metal nanoparticle results in both hot electron generation and photothermal heating[6 66,67] due to nonradiative energy transfer processes, such as electron-phonon coupling in the metal. Both processes can simultaneously play a critical role in driving chemical reactions (resonant energy transfer and radiative processes[33] may also occur but are not the focus of this article). To understand which fundamental processes are occurring in plasmonic photocatalysis, it is important to monitor the reaction temperature at the photocatalyst surface to elucidate the relative role of electron- and phonon-driven processes in the overall chemical reaction.

In a recent study of ammonia decomposition using a plasmonic photocatalyst,[68] the relationship between thermal and electronic excitations was addressed by introducing the concept of a light-dependent activation barrier, to account for the effect of light illumination on both electronic and thermal excitations within the same unified framework (Fig. 9). In this study an antenna-reactor particle of a new geometry was developed, namely a Cu nanoparticle with a Cu-Ru surface alloy. The surface stoichiometry was such that the presence of Ru on the surface did not appreciably compromise or dampen the plasmonic response of the Cu nanoparticle. The Cu-Ru antenna reactor-nanoparticles were dispersed within a MgO support matrix (Fig. 9(A)). Ru was chosen as the reactor site because of its affinity for reversible binding of nitrogen-containing molecules, such as ammonia. The Cu-Ru antenna-reactor nanoparticle was found to be substantially more photocatalytically active than either Cu or Ru nanoparticles alone, and substantially more photocatalytically than thermocatalytically active (Fig. 9(B)). The ammonia decomposition reaction was monitored by measuring the H_2 product generation rate under both thermocatalytic and photocatalytic conditions (Fig. 9(C)). Here it is important to note that the photocatalytic reaction can produce the same rate of ammonia decomposition as the thermocatalytic reaction but at a substantially lower temperature.[69] In both cases the surface temperature was monitored using an infrared-detecting thermometer with temperatures that were found to be in excellent agreement with theoretical simulations. Illumination of the photocatalyst also increases its surface temperature due to photothermal heating: the question is how to quantify these two contributions. By measuring the Arrhenius dependence of the photocatalytic reaction on surface temperature of the catalyst, under conditions of illumination alone and combined with carefully controlled thermal heating and monitoring, the reaction barrier was found to be reduced under illumination conditions of both wavelength and intensity. Expressing this behavior in the form of a light-induced reaction barrier allows one to clearly quantify the photonic versus thermal contributions. For example, if this reaction was exclusively photothermal in nature with no hot electron contributions, the slope of the Arrhenius plot would not change with illumination intensity or wavelength. Any change in slope due to illumination

intensity shows that processes other than purely thermal ones are also contributing to the chemical reaction. For ammonia decomposition, this light-reduced reaction barrier is plotted as a function of both laser power and wavelength (Fig. 9(D)). The reaction barrier for the purely thermocatalytic reaction is shown at the right of this contour plot, corresponding to zero illumination intensity. The reaction barrier upon illumination is reduced, with both a wavelength and a laser power dependence. The barrier reduction is maximum at the illumination wavelength of 550 nm, which corresponds to the spectral peak of the plasmon resonance of the Cu-Ru antenna-reactor particle. For ammonia decomposition with this antenna-reactor photocatalyst, the reaction barrier is reduced from 1.2 eV to 0.2 eV at the optimal wavelength (Fig. 9(D)). This large reduction in reaction barrier changes the rate-limiting step in this well-studied reaction: the reaction coordinate for ammonia decomposition is shown in Figure 9(E). Under thermocatalytic conditions, the rate-limiting step for this reaction is the associative desorption of N_2 from the Ru reactive sites. For the photocatalyzed reaction, the hot electrons generated by plasmon decay contribute to a desorption of the N_2 from the photocatalyst surface (Fig. 9(F), similar to the photoinduced desorption discussed earlier in the case of acetylene hydrogenation and enhanced ethylene/ethane specificity (Fig. 7(C)). [60]

Outlook

The exciting results shown to date in the case of hot electron photodetection could potentially alter the way that photodetectors are envisions, and in nascent field of plasmonic photocatalysis could lead to a revolution in chemistry and in the chemical industry. Conventional chemical processes that require high temperatures and pressures also require substantial capital investments and benefit from an economy of scale: these practices have given rise to the large chemical processing plants that are the industry standard. Can these new photon-driven ways of doing chemistry be translated into industrial processes that rely on photons-either sunlight or inexpensive, high efficiency photon sources that are currently available- for energy? To translate this work into industrial practice will require a complete change of both education and mindset for chemical engineers, and may result in the establishment of a new field of "photocatalysis engineer" to fully translate these new ideas into real-world applications.

Acknowledgements

I would like to thank the many students, postdocs, and collaborators whom I have worked with on these topics in the past years. I would also like to thank the funding agencies that have supported this work: The Air Force Office of Scientific Research, the Office of Naval Research, the Army Research Office, the Defense Threat Reduction Agency, the National Science Foundation (all U. S.), and the Welch Foundation for their ongoing and generous support. In particular, I would like to thank my main collaborator in these efforts, Peter Nordlander, for critical reading of this manuscript.

References

1 Bohren, C. F. How can a particle absorb more than the light incident on it. *Am. J. Phys.* **51**, 323-327, doi:10.1119/1.13262 (1983).

2 Lindquist, N. C., Nagpal, P., McPeak, K. M., Norris, D. J. & Oh, S. H. Engineering metallic nanostructures for plasmonics and nanophotonics. *Reports on Progress in Physics* **75**, doi:10.1088/0034-4885/75/3/036501 (2012).

3 Maier, S. A. & Atwater, H. A. Plasmonics: Localization and guiding of electromagnetic energy in metal/dielectric structures. *Journal of Applied Physics* **98**, doi:10.1063/1.1951057 (2005).

4 Pelton, M., Aizpurua, J. & Bryant, G. Metal-nanoparticle plasmonics. *Laser & Photonics Reviews* **2**, 136-159, doi:10.1002/lpor.200810003 (2008).

5 Stockman, M. I. Nanoplasmonics: past, present, and glimpse into future. *Opt. Express* **19**, 22029-22106, doi:10.1364/oe.19.022029 (2011).

6 Baffou, G. & Quidant, R. Thermo-plasmonics: using metallic nanostructures as nano-sources of heat. *Laser & Photonics Reviews* **7**, 171-187, doi:10.1002/lpor.201200003 (2013).

7 Biagioni, P., Huang, J. S. & Hecht, B. Nanoantennas for visible and infrared radiation. *Reports on Progress in Physics* **75**, doi:10.1088/0034-4885/75/2/024402 (2012).

8 Chen, H. J., Shao, L., Li, Q. & Wang, J. F. Gold nanorods and their plasmonic properties. *Chemical Society Reviews* **42**, 2679-2724, doi:10.1039/c2cs35367a (2013).

9 Eustis, S. & El-Sayed, M. A. Why gold nanoparticles are more precious than pretty gold: Noble metal surface plasmon resonance and its enhancement of the radiative and nonradiative properties of nanocrystals of different shapes. *Chemical Society Reviews* **35**, 209-217, doi:10.1039/b514191e (2006).

10 Huang, X. H., Neretina, S. & El-Sayed, M. A. Gold Nanorods: From Synthesis and Properties to Biological and Biomedical Applications. *Advanced Materials* **21**, 4880-4910, doi:10.1002/adma.200802789 (2009).

11 Gramotnev, D. K. & Bozhevolnyi, S. I. Plasmonics beyond the diffraction limit. *Nat. Photonics* **4**, 83-91, doi:10.1038/nphoton.2009.282 (2010).

12 Bao, Q. L. & Loh, K. P. Graphene Photonics, Plasmonics, and Broadband Optoelectronic Devices. *ACS Nano* **6**, 3677-3694, doi:10.1021/nn300989g (2012).

13 Dieterich, J. M. & Carter, E. A. Quantum solutions for a sustainable energy future. *Nat. Rev. Chem.* **1**, doi:10.1038/s41570-017-0032 (2017).

14 Halas, N. J., Lal, S., Chang, W. S., Link, S. & Nordlander, P. Plasmons in Strongly Coupled Metallic Nanostructures. *Chemical Reviews* **111**, 3913-3961, doi:10.1021/cr200061k (2011).

15 Lal, S., Link, S. & Halas, N. J. Nano-optics from sensing to waveguiding. *Nat. Photonics* **1**, 641-648, doi:10.1038/nphoton.2007.223 (2007).

16 Zheludev, N. I. & Kivshar, Y. S. From metamaterials to metadevices. *Nature Materials* **11**, 917-924, doi:10.1038/nmat3431 (2012).

17 Willets, K. A. & Van Duyne, R. P. Localized surface plasmon resonance spectroscopy and sensing. *Annual Review of Physical Chemistry* **58**, 267-297, doi:10.1146/annurev.physchem.58.032806.104607 (2007).

18 Anker, J. N. *et al.* Biosensing with plasmonic nanosensors. *Nature Materials* **7**, 442-453, doi:10.1038/nmat2162 (2008).

19 Homola, J. Present and future of surface plasmon resonance biosensors. *Analytical and Bioanalytical Chemistry* **377**, 528-539, doi:10.1007/s00216-003-2101-0 (2003).

20 Hutter, E. & Fendler, J. H. Exploitation of localized surface plasmon resonance. *Advanced Materials* **16**, 1685-1706, doi:10.1002/adma.200400271 (2004).

21 Vollmer, F. & Arnold, S. Whispering-gallery-mode biosensing: label-free detection down to single molecules. *Nature Methods* **5**, 591-596, doi:10.1038/nmeth.1221 (2008).

22 Aitchison, H. *et al.* Analytical SERS: general discussion. *Faraday Discussions* **205**, 561-600, doi:10.1039/c7fd90096a (2017).

23 Aizpurua, J. *et al.* Ultrasensitive and towards single molecule SERS: general discussion. *Faraday Discussions* **205**, 291-330, doi:10.1039/c7fd90088k (2017).

24 Cialla, D. *et al.* Surface-enhanced Raman spectroscopy (SERS): progress and trends. *Analytical and Bioanalytical Chemistry* **403**, 27-54, doi:10.1007/s00216-011-5631-x (2012).

25 Graham, D. *et al.* Theory of SERS enhancement: general discussion. *Faraday Discussions* **205**, 173-211, doi:10.1039/c7fd90095c (2017).

26 Henry, A. I., Ueltschi, T. W., McAnally, M. O. & Van Duyne, R. P. Spiers Memorial Lecture Surface-enhanced Raman spectroscopy: from single particle/molecule spectroscopy to angstrom-scale spatial resolution and femtosecond time resolution. *Faraday Discussions* **205**, 9-30, doi:10.1039/c7fd00181a (2017).

27 Stiles, P. L., Dieringer, J. A., Shah, N. C. & Van Duyne, R. R. Surface-Enhanced Raman Spectroscopy. *Annual Review of Analytical Chemistry* **1**, 601-626, doi:10.1146/annurev.anchem.1.031207.112814 (2008).

28 Baker, G. A. & Moore, D. S. Progress in plasmonic engineering of surface-enhanced Raman-scattering substrates toward ultra-trace analysis. *Analytical and Bioanalytical Chemistry* **382**, 1751-1770, doi:10.1007/s00216-005-3353-7 (2005).

29 Atwater, H. A. & Polman, A. Plasmonics for improved photovoltaic devices. *Nature Materials* **9**, 205-213, doi:10.1038/nmat2629 (2010).

30 Pillai, S. & Green, M. A. Plasmonics for photovoltaic applications. *Solar Energy Materials and Solar Cells* **94**, 1481-1486, doi:10.1016/j.solmat.2010.02.046 (2010).

31 Gan, Q. Q., Bartoli, F. J. & Kafafi, Z. H. Plasmonic-Enhanced Organic Photovoltaics: Breaking the 10% Efficiency Barrier. *Advanced Materials* **25**, 2385-2396, doi:10.1002/adma.201203323 (2013).

32 Guo, C. F., Sun, T. Y., Cao, F., Liu, Q. & Ren, Z. F. Metallic nanostructures for light trapping in energy-harvesting devices. *Light-Science & Applications* **3**, doi:10.1038/lsa.2014.42 (2014).

33 Cai, Y.-Y. *et al.* Photoluminescence of Gold Nanorods: Purcell Effect Enhanced Emission from Hot Carriers. *ACS Nano* **12**, 976-985 (2018).

34 Liu, J. G., Zhang, H., Link, S. & Nordlander, P. Relaxation of Plasmon-Induced Hot Carriers. *ACS Photonics* **5**, 2584-2595 (2018).

35 Clavero, C. Plasmon-induced hot-electron generation at nanoparticle/metal-oxide interfaces for photovoltaic and photocatalytic devices. *Nat. Photonics* **8**, 95-103, doi:10.1038/nphoton.2013.238 (2014).

36 Brongersma, M. L., Halas, N. J. & Nordlander, P. Plasmon-induced hot carrier science and technology. *Nature Nanotechnology* **10**, 25-34, doi:10.1038/nnano.2014.311 (2015).

37 Manjavacas, A., Liu, J. G., Kulkarni, V. & Nordlander, P. Plasmon-Induced Hot Carriers in Metallic Nanoparticles. *ACS Nano* **8**, 7630-7638, doi:10.1021/nn502445f (2014).

38 Dorodnyy, A. *et al.* Plasmonic Photodetectors. *IEEE J. Sel. Top. Quantum Electron.* **24**, doi:10.1109/jstqe.2018.2840339 (2018).

39 Knight, M. W., Sobhani, H., Nordlander, P. & Halas, N. J. Photodetection with Active Optical Antennas. *Science* **332**, 702-704, doi:10.1126/science.1203056 (2011).

40 Knight, M. W. *et al.* Embedding Plasmonic Nanostructure Diodes Enhances Hot Electron Emission. *Nano Letters* **13**, 1687-1692, doi:10.1021/nl400196z (2013).

41 Sobhani, A. *et al.* Narrowband photodetection in the near-infrared with a plasmon-induced hot electron device. *Nature Communications* **4**, doi:10.1038/ncomms2642 (2013).

42 Zheng, B. Y. *et al.* Distinguishing between plasmon-induced and photoexcited carriers in a device geometry. *Nature Communications* **6**, doi:10.1038/ncomms8797 (2015).

43 Fang, Z. Y. *et al.* Graphene-Antenna Sandwich Photodetector. *Nano Letters* **12**, 3808-3813, doi:10.1021/nl301774e (2012).

44 Zuloaga, J., Prodan, E. & Nordlander, P. Quantum Plasmonics: Optical Properties and Tunability of Metallic Nanorods. *ACS Nano* **4**, 5269-5276 (2010).

45 Mukherjee, S. *et al.* Hot Electrons Do the Impossible: Plasmon-Induced Dissociation of H-2 on Au. *Nano Letters* **13**, 240-247, doi:10.1021/nl303940z (2013).

46 Fan, J. A. *et al.* Self-Assembled Plasmonic Nanoparticle Clusters. *Science* **328**, 1135-1138, doi:10.1126/science.1187949 (2010).

47 Tanzid, M. *et al.* Combining Plasmonic Hot Carrier Generation with Free Carrier Absorption for High-Performance Near-Infrared Silicon-Based Photodetection. *ACS Photonics* **5**, 3472-3477, doi:10.1021/acsphotonics.8b00623 (2018).

48 Cortes, E. Activating plasmonic chemistry. *Science* **362**, 28-29, doi:10.1126/science.aav1133 (2018).

49 Lee, J., Mubeen, S., Ji, X. L., Stucky, G. D. & Moskovits, M. Plasmonic Photoanodes for Solar Water Splitting with Visible Light. *Nano Letters* **12**, 5014-5019, doi:10.1021/nl302796f (2012).

50 Silva, C. G., Juarez, R., Marino, T., Molinari, R. & Garcia, H. Influence of Excitation Wavelength (UV or Visible Light) on the Photocatalytic Activity of Titania Containing Gold Nanoparticles for the Generation of Hydrogen or Oxygen from Water. *Journal of the American Chemical Society* **133**, 595-602, doi:10.1021/ja1086358 (2011).

51 Ingram, D. B. & Linic, S. Water Splitting on Composite Plasmonic-Metal/Semiconductor Photoelectrodes: Evidence for Selective Plasmon-Induced Formation of Charge Carriers near the Semiconductor Surface. *Journal of the American Chemical Society* **133**, 5202-5205, doi:10.1021/ja200086g (2011).

52 Murdoch, M. *et al.* The effect of gold loading and particle size on photocatalytic hydrogen production from ethanol over Au/TiO2 nanoparticles. *Nature Chemistry* **3**, 489-492, doi:10.1038/nchem.1048 (2011).

53 Seh, Z. W. *et al.* Janus Au-TiO2 Photocatalysts with Strong Localization of Plasmonic Near-Fields for Efficient Visible-Light Hydrogen Generation. *Advanced Materials* **24**, 2310-2314, doi:10.1002/adma.201104241 (2012).

54 Christopher, P., Xin, H. L. & Linic, S. Visible-light-enhanced catalytic oxidation reactions on plasmonic silver nanostructures. *Nature Chemistry* **3**, 467-472, doi:10.1038/nchem.1032 (2011).

55 Hung, W. H., Aykol, M., Valley, D., Hou, W. B. & Cronin, S. B. Plasmon Resonant Enhancement of Carbon Monoxide Catalysis. *Nano Letters* **10**, 1314-1318, doi:10.1021/nl9041214 (2010).

56 Hou, W. B. *et al.* Photocatalytic Conversion of CO2 to Hydrocarbon Fuels via Plasmon-Enhanced Absorption and Metallic Interband Transitions. *Acs Catalysis* **1**, 929-936, doi:10.1021/cs2001434 (2011).

57 Mukherjee, S. *et al.* Hot-Electron-Induced Dissociation of H-2 on Gold Nanoparticles Supported on SiO2. *Journal of the American Chemical Society* **136**, 64-67, doi:10.1021/ja411017b (2014).

58 Zhou, L. *et al.* Aluminum Nanocrystals as a Plasmonic Photocatalyst for Hydrogen Dissociation. *Nano Letters* **16**, 1478-1484, doi:10.1021/acs.nanolett.5b05149 (2016).

59 McClain, M. J. *et al.* Aluminum Nanocrystals. *Nano Letters* **15**, 2751-2755, doi:10.1021/acs.nanolett.5b00614 (2015).

60 Swearer, D. F. *et al.* Heterometallic antenna-reactor complexes for photocatalysis. *Proceedings of the National Academy of Sciences of the United States of America* **113**, 8916-8920, doi:10.1073/pnas.1609769113 (2016).

61 Swearer, D. F. *et al.* Transition-Metal Decorated Aluminum Nanocrystals. *ACS Nano* **11**, 10281-10288, doi:10.1021/acsnano.7604960 (2017).
62 Zhang, C. *et al.* Al-Pd Nanodisk Heterodimers as Antenna-Reactor Photocatalysts. *Nano Letters* **16**, 6677-6682, doi:10.1021/acs.nanolett.6b03582 (2016).
63 Dong, W. & Hafner, J. H_2 dissociative adsorption on Pd(111). *Phys. Rev. B* **56**, 15396–15403 (1997).
64 Mitsui, T., Rose, M. K., Fomin, E., Ogletree, D. F. & Salmeron, M. Dissociative hydrogen adsorption on Pd requires aggregates of three or more vacancies. *Nat. Catal.* **422**, 705-707 (2003).
65 Linic, S., Aslam, U., Boerigter, C. & Morabito, M. Photochemical transformations on plasmonic metal nanoparticles. *Nature Materials* **14**, 567-576 (2015).
66 Hirsch, L. R. *et al.* Nanoshell-mediated near-infrared thermal therapy of tumors under magnetic resonance guidance. *Proceedings of the National Academy of Sciences of the United States of America* **100**, 13549-13554, doi:10.1073/pnas.2232479100 (2003).
67 Hogan, N. J. *et al.* Nanoparticles Heat through Light Localization. *Nano Letters* **14**, 4640-4645, doi:10.1021/nl5016975 (2014).
68 Zhou, L. A. *et al.* Quantifying hot carrier and thermal contributions in plasmonic photocatalysis. *Science* **362**, 69-+, doi:10.1126/science.aat6967 (2018).
69 Martirez, J. M. P. & Carter, E. A. Prediction of a low-temperature N-2 dissociation catalyst exploiting near-IR-to-visible light nanoplasmonics. *Sci. Adv.* **3**, doi:10.1126/sciadv.aao4710 (2017).